Inorganic Chemistry

Article

pubs.acs.org/IC

Time-Resolved Assembly of Chiral Uranyl Peroxo Cage Clusters Containing Belts of Polyhedra

Jie Qiu,[†] Kevin Nguyen,[‡] Laurent Jouffret,[†] Jennifer E. S. Szymanowski,[†] and Peter C. Burns*[,†,‡]

[†]Department of Civil and Environmental Engineering and Earth Sciences, University of Notre Dame, Notre Dame, Indiana 46556, United States

[‡]Department of Chemistry and Biochemistry, University of Notre Dame, Notre Dame, Indiana 46556, United States

Supporting Information

ABSTRACT: Two chiral cage clusters built from uranyl polyhedra and $(HPO_3)^{2-}$ groups have been synthesized in pure yield and characterized structurally and spectroscopically in the solid state and aqueous solution. Synthesis reactions under ambient conditions in mildly acidic aqueous solutions gave clusters $U_{22}PO_3$ and $U_{28}PO_3$ that contain belts of four uranyl peroxide pentagonal and hexagonal bipyramids, in contrast to earlier reported uranyl peroxide cage clusters that are built from four-, five-, and six-membered rings of uranyl hexagonal bipyramids. $U_{22}PO_3$ and $U_{28}PO_3$ are also the first chiral uranyl-based cage clusters, the first that contain uranyl pentagonal bipyramids that contain no peroxide ligands, and the first that incorporate $(HPO_3)^{2-}$ bridges between uranyl ions. They are built from 22 uranyl polyhedra and 20 $(HPO_3)^{2-}$ groups, or 28 uranyl polyhedra and 24 $(HPO_3)^{2-}$ groups, with the outer and inner surfaces of the cages passivated by the O atoms of uranyl ions. Small-angle X-ray scattering (SAXS) profiles demonstrated that $U_{22}PO_3$ clusters formed in solution within 1 h after mixing of reactants, and remained in solution for 2 weeks prior to crystallization. Time-resolved electrospray ionization mass spectrometry and SAXS demonstrated that $U_{28}PO_3$ clusters formed in solution within 1 h of mixing the reactants, and remained in solution 1 month before crystallization. Crystallization of $U_{22}PO_3$ and $U_{28}PO_3$ is accelerated by addition of KNO_3. Clusters of $U_{22}PO_3$ with and without encapsulated cations exhibit markedly different aqueous solubility, reflecting the importance of cluster surface charge in fostering linkages through counterions to form a stable solid.

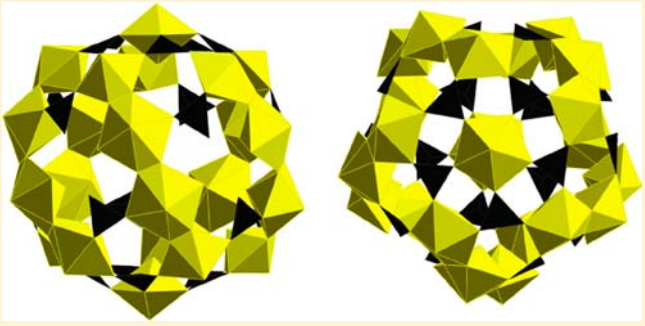

1. INTRODUCTION

Polyoxometalates (POMs), a subset of metal oxide clusters, exhibit diverse compositions and nanoscale architectures, as well as unusual optical, catalytic, and magnetic properties with emerging important applications.[1−6] They provide ideal systems to study the behavior of nanomaterials with well-defined structures.[7] In contrast to the extensive investigations of transition-metal oxide clusters,[1−5,7] studies of actinide oxide clusters are at an early stage and most have focused on the synthesis and structures of uranyl-based clusters. However, control of actinide materials at the nanoscale holds considerable promise for applications in an advanced nuclear energy system, including in the fabrication of new fuels and separation of radionuclides during recycling. Actinide clusters may also be useful models for understanding geochemical reactions and are potential candidates in the design of catalysts and molecular magnets.[8]

Synthesis of finite clusters built of metal cations and oxygen in solution requires surface passivation,[9,10] which may be accomplished using appropriate inorganic[11] or organic[8,12−14] ligands, and by incorporating cations with "yl" oxygen atoms.[1,15] The "yl" oxygen atom is doubly or triply bonded to the corresponding metal cation, and thus tends not to form additional strong bonding interactions.[16] By passivation of the surface of actinide oxide clusters using ligands, clusters containing cores consisting of 6 Th (IV),[13,17−19] U (IV and/or V),[12,13,19−24] or Pu (IV);[18,19] 8 U (IV);[14,26] 10 U (IV);[8] 12 U (IV and V);[24] 16 U (IV and V);[8] or 38 Pu (IV)[11] cations have been crystallized. Using the "yl" atoms of the linear dioxo uranyl cation $(UO_2)^{2+}$ for cluster surface passivation, more than 35 unique nanoscale cage clusters containing up to 120 uranyl cations have been synthesized in aqueous solution under ambient conditions.[27−40] Whereas uranyl ions contained in bipyramidal polyhedra typically link into extended structures, especially infinite sheets,[41−43] where the uranyl ions are bridged by bidentate peroxo ligands, bent U−(O_2)−U dihedral angles are favored and appear to foster the assembly of cage clusters.[44,45]

Uranyl peroxide cage clusters are constructed from only uranyl polyhedra, as well as with oxalate, nitrate, pyrophosphate, or methylenediphosphonate bridges, and can form over a broad range of pH conditions. Counterions impact the size of the clusters by adjusting the U−(O_2)−U dihedral angles,[44,45]

Received: September 25, 2012
Published: December 11, 2012

   dx.doi.org/10.1021/ic3020817 | *Inorg. Chem.* 2013, 52, 337−345

and high-symmetry isomers are generally preferred.[33,35] Most significantly, from the perspective of the current contribution, all of these clusters are built from combinations of four-, five-, or six-membered rings of uranyl polyhedra, which correspond to topological squares, pentagons, and hexagons that are stabilized by different counterions.[44] This limits the pore sizes of these clusters and restricts their topologies to a family of three-connected graphs. Where oxalate, pyrophosphate, or methylenediphosphonate bridges are present, they bridge between uranyl polyhedra with a "side-on" bidentate configuration, which is topologically analogous to the direct sharing of equatorial edges between uranyl polyhedra.[29−31]

Members of the family of uranyl peroxide clusters are synthesized by one-pot reactions, and it is difficult to identify specific reaction pathways of the self-assembly processes in solution, or even to characterize the initial occurrence of the clusters in solution.[29] Only limited insights are available concerning the mechanisms and kinetics of the formation of such clusters.[27,38]

In an attempt to derive unique cluster topologies with tunable properties, we have used C_{3v} $(HPO_3)^{2-}$ anions as bridging ligands because it is unlikely for them to bridge between two uranyl polyhedra with the ligand bidentate to each uranyl ion. Cage clusters employing this type of bridge between uranyl ions must be topologically distinct from those found in our earlier studies. Several actinide phosphites with extended structures have been synthesized under hydrothermal conditions,[46−50] but uranyl cage clusters with these ligands have not been explored. A one-pot repeatable synthesis reaction provides for the crystallization of two different pairs of chiral cage clusters. These are designated $U_{22}PO_3$ and $U_{28}PO_3$ and possess novel building units and topologies. They are also the first chiral uranyl peroxide clusters. We report their synthesis, characterization, and their assembly in solution as studied by time-resolved electrospray ionization mass spectrometry (ESI-MS) and small-angle X-ray scattering (SAXS).

2. EXPERIMENTAL METHODS

2.1. Synthesis of Clusters $U_{22}PO_3$ and $U_{28}PO_3$. *Caution! Although depleted uranium was used in these experiments, it is radioactive and toxic and should only be handled by qualified personnel in appropriate facilities.*

The synthesis of clusters of uranyl peroxide polyhedra containing $(HPO_3)^{2-}$ groups is only possible if oxidation of $(HPO_3)^{2-}$ by peroxide is avoided, or at least is slower than cluster assembly. Here, we used the K salt of EDTA, which is partially oxidized in our aqueous systems in the presence of peroxide,[51] to effectively prevent the oxidation of $(HPO_3)^{2-}$.

A single synthesis reaction produced two types of crystals at room temperature, one containing a pair of $U_{22}PO_3$ clusters and the other a pair of $U_{28}PO_3$ clusters (Figure S1, Supporting Information). They were synthesized by loading aqueous solutions of $UO_2(NO_3)_2{\cdot}6H_2O$ (0.5 M, 1 mL), H_2O_2 (30%, 1 mL), tetraethylammonium hydroxide (TEAH, 40%, 1 mL), H_3PO_3 (0.5 M, 3.0 mL), and ethylenediaminetetraacetic acid dipotassium salt (EDTA-K_2, 0.5 M, 0.5 mL) to a 20 mL glass vial. The vial was shaken, giving a homogeneous cloudy solution with a pH of ∼6.0. After 1 week, this mixture was centrifuged in a 50 kDa Amicon centrifugal filter and the filtrate was transferred to a new 20 mL glass vial. Light yellow block-shaped crystals containing the $U_{22}PO_3$ cluster appeared in a week with the solution left to evaporate under ambient conditions. Subsequent to the crystallization of $U_{22}PO_3$, the remaining clear solution was transferred to a new glass vial and was left to evaporate under ambient conditions. After 2 weeks, yellow block-shaped crystals containing the $U_{28}PO_3$ cluster formed. Clusters containing $U_{22}PO_3$ or $U_{28}PO_3$ obtained from this synthesis method contain K countercations (see section 3.3) and are hereafter designated as $K\_U_{22}PO_3$ and $K\_U_{28}PO_3$. The yields of $K\_U_{22}PO_3$ and $K\_U_{28}PO_3$ crystals were ∼10% and ∼35%, respectively, on the basis of uranium.

We found that repeating the above-described synthesis reaction with the addition of ∼0.05 g of KNO_3 reduced the time to crystallization of $K\_U_{22}PO_3$ to 3 days, whereas addition of ∼0.15 g of KNO_3 gave crystals of $K\_U_{28}PO_3$ within 3 days. For the first case, $K\_U_{28}PO_3$ clusters subsequently crystallized within about 2 weeks after crystallization of $K\_U_{22}PO_3$ clusters. For the second case, addition of ∼0.15 g of KNO_3 caused immediate formation of a fine-grained precipitate of $K\_U_{22}PO_3$. The yields were not noticeably improved in either case. Repeating the synthesis reaction described above with the addition of ∼0.1 g of $NaNO_3$ provided crystals of $U_{22}PO_3$ clusters with Na^+, K^+, and tetraethylammonium countercations (see section 3.3), which are hereafter designated as $NaK\_U_{22}PO_3$. The yield of $NaK\_U_{22}PO_3$ crystals remained about the same as that for $K\_U_{22}PO_3$, although the addition of $NaNO_3$ resulted in larger crystals.

The reproducibility of the synthesis products described above is excellent, as the synthesis reactions were repeated dozens of times to accumulate sufficient material for characterization and ongoing experiments to be reported elsewhere. The synthesis reactions were found to be sensitive to solution pH, with crystals obtained for pH in the range of 5.2−6.5, as adjusted using a combination of TEAH, H_3PO_3, and EDTA-K_2. Visually superior crystals resulted for a pH of ∼6.

2.2. Single-Crystal X-ray Diffraction. Structure determinations for crystals containing nanoscale clusters of uranyl polyhedra are difficult because of the contrast between U and the lighter elements present, the presence of relatively large void spaces, and disorder of the counterions and H_2O both inside and between the clusters. Despite these limitations, details of the structural connectivities of the uranyl-based clusters are uniquely attainable through X-ray diffraction.[6]

Crystals were placed on cryo-loops in oil and cooled to 100 K for data collection using a Bruker APEX II diffractometer equipped with monochromated Mo $K\alpha$ X-radiation provided by a conventional sealed tube. A sphere of data was collected for each crystal using frame widths of 0.5° in ω. Data were corrected for Lorentz, polarization, and background effects using the Bruker APEX II software, and semiempirical corrections for absorption were performed using SADABS.[52] Structure solutions and refinements were done with SHELXTL.[53] The structure determinations for $NaK\_U_{22}PO_3$ and $K\_U_{28}PO_3$ were relatively straightforward, although positional disorder of H_2O groups, K^+, and/or Na^+cations are complicating factors. The crystal of $K\_U_{22}PO_3$ contained two domains, although optical examination did not reveal their presence. The refinement included these two domains, and their refined ratios were 0.76:0.24. Diffraction data were collected for several crystals corresponding to each cluster, with the superior results reported here. Crystallographic parameters and refinement details are provided in the Supporting Information.

The crystal-structure analysis of each cluster revealed the presence of different types of O atoms. Those of the uranyl dioxo cations were readily apparent because each forms one bond to U^{6+} at ∼1.8 Å. O atoms of peroxo groups were indicated by O−O bond lengths of ∼1.5 Å. O atoms that occur at an equatorial position of a uranyl hexagonal bipyramid and that are bonded to a single U^{6+} cation at a distance of ∼2.4 Å are H_2O, by analogy with many solid-state structures.[42] Oxygen atoms of $(HPO_3)^{2-}$ groups are readily assigned because of their bond to P^{3+} as well as U^{6+} cations. Bond-valence analysis confirmed each of the assignments designated here.[54]

2.3. Chemical Analysis. *U, P, Na, and K Analysis.* Crystals of each cluster were separately removed from their corresponding glass vial, vacuum filtered using a Whatman1 filter membrane, and rinsed with 100 mL of ethanol. About 10 mg of material was recovered in each case and was dissolved in 0.5 mL of concentrated HNO_3. The resulting solutions were added to 5% (v/v) HNO_3 to produce 10 mL samples for analyses of U, P, and K that contained 1−20 ppm of the cations. Samples were analyzed using a Perkin-Elmer inductively coupled plasma optical emission spectrometer (ICP-OES).

dx.doi.org/10.1021/ic3020817 | Inorg. Chem. 2013, 52, 337−345

C and N Analysis. Crystals were isolated and rinsed with ethanol and were then placed in a 5 mL glass vial in a desiccator overnight to remove surface water. Crystals were analyzed using a Costech elemental analyzer (ECS 4010).

2.4. Small-Angle X-ray Scattering. Small-angle X-ray scattering (SAXS) data were collected using a Bruker Nanostar instrument equipped with a Cu microfocus source, Montel multilayer optics, and a HiSTAR multiwire detector. Data were collected with a sample-to-detector distance of 26.3 cm and the sample chamber under vacuum.

Crystals containing clusters for analysis by SAXS were isolated from their mother solution by vacuum filtration, rinsed with water, and harvested from the filter membrane. In each case, about 11 mg of crystals was dissolved in 1.0 mL of aqueous solution. Pure $K\_U_{22}PO_3$ crystals and a mixture of $K\_U_{22}PO_3$ and $K\_U_{28}PO_3$ crystals (in proportion to their synthesis yields) were dissolved in aliquots of 0.1 M Na_2HPO_3 solution. Pure $NaK\_U_{22}PO_3$ and $K\_U_{28}PO_3$ crystals were dissolved in ultrapure water. The resulting solutions were placed in 0.5 mm diameter glass capillaries, the ends of which were sealed using wax. Water was placed in an identical capillary for measurement of the background.

Following preparation of the synthesis reactions described above, aliquots of the solutions were collected at various times for subsequent collection of SAXS data. These solutions were centrifuged in a 50 kDa Amicon centrifugal filter, and filtrates were placed in glass capillaries for SAXS data collection, as described above.

2.5. Electrospray Ionization Mass Spectrometry. ESI-MS spectra[55] were collected in negative-ion mode using a Bruker micrOTOF-Q II high-resolution quadrapole time-of-flight (Q-TOF) spectrometer (3600 V capillary voltage, 0.8 bar nebulizer gas, 4 L/min dry gas, 180 °C dry gas temperature). The solutions measured were diluted to about 50−100 ppm U and were introduced by direct infusion at 7 μL/min and scanned over a 500−5000 m/z range with data averaged over 5 min. Data were deconvoluted using the MaxEnt software.

Two groups of specimens were prepared for collection of ESI-MS data. One suite was produced by dissolving crystals in a 50 μL aqueous solution. Crystals were isolated and rinsed by water prior to their dissolution. $K\_U_{22}PO_3$ crystals were dissolved in 1 mM Na_2HPO_3 solution, and $K\_U_{28}PO_3$ crystals were dissolved in ultrapure water. The resulting solutions were then diluted 10-fold using ultrapure water. The second suite of samples was reaction solutions collected over time, prior to formation of crystals of $K\_U_{28}PO_3$. For each sample, 500 μL of the reaction solution was filtered using a Millex PTFE syringe filter with a pore size of 0.2 μm. The filtrate was centrifuged in a 3 kDa Amicon centrifugal filter, rinsed with 400 μL of water, and centrifuged three times. The solution was subsequently diluted 1000-fold by adding ultrapure water. ESI-MS spectra were collected immediately following sample preparation.

2.6. Thermogravimetric Analysis. Thermogravimetric analysis (TGA) measurements were done using a Netzsch TG209 F1 Iris thermal analyzer for crystals in Al crucibles under flowing nitrogen gas. Harvested crystals were heated from 20 to 100 °C at a rate of 5 °C/min and were then held at 105 °C for 30 min. The remaining material was then heated to 550 °C at a rate of 5 °C/min. The masses of $K\_U_{22}PO_3$, $NaK\_U_{22}PO_3$, and $K\_U_{28}PO_3$ crystals used were 15.04, 12.58, and 12.91 mg, respectively. The specimens lost 14, 17, and 16% of their masses by 550 °C. Data are given in Figure S6 (Supporting Information).

2.7. Spectroscopic Characterization. Infrared spectra were collected for single crystals of $K\_U_{22}PO_3$, $NaK\_U_{22}PO_3$, and $K\_U_{28}PO_3$, as well as their TGA residues, using a SensIR technology IlluminatIR FT-IR microspectrometer. A single crystal (or powder of TGA residue) was placed on a glass slide for data collection. The spectra were measured from 650 to 4000 cm^{-1} with a beam aperture of 100 μm using a diamond-tipped ATR objective. The spectra collected from single crystals, given in Figure S7 (Supporting Information), confirm the presence of $(HPO_3)^{2-}$, uranyl ions, tetraethylammonium, and H_2O groups. Uranyl ion stretches occur at ∼850 cm^{-1}, $(HPO_3)^{2-}$ and C−N modes are in the range of ∼1000−1100 cm^{-1}, modes in the range of ∼1300−1500 cm^{-1} are attributed to the tetraethylammonium cations, a H_2O bending mode is at ∼1680 cm^{-1}, and O−H bonds are indicated by the broad envelope from about 2600 to 3600 cm^{-1}. The spectra collected from the TGA residues indicate that H_2O, OH^-, and tetraethylammonium groups were lost during the TGA measurement.

Raman spectra for a 40% TEAH solution, for reaction solutions collected both 3 days and 3 months after mixing (with the 3 month solution in a capped vial to prevent evaporation and crystallization), and for standard solutions of Na_2HPO_4 and Na_2HPO_3 were collected using a Bruker Sentinel system linked via fiber optics to a Raman probe equipped with a 785 nm, 400 mW laser and a high-sensitivity, TE-cooled, 1024 × 255 CCD array. The spectra were collected for 15 s with three signal accumulations, in the range from 80 to 3200 cm^{-1}. The spectra of $K\_U_{22}PO_3$, $NaK\_U_{22}PO_3$, and $K\_U_{28}PO_3$ crystals were also collected with the same instrument connected to a microscope mount, with a video-assisted fiber optic probe. The spectra were collected from 80 to 3200 cm^{-1} for 5 s with five signal accumulations. All spectra are in the Supporting Information. The Raman spectrum of each crystal displays intense bands around 805 and 870 cm^{-1} (Figure S8, Supporting Information). The UO_2 stretch is at 814, 816, and 808 cm^{-1} for $K\_U_{22}PO_3$, $NaK\_U_{22}PO_3$, and $K\_U_{28}PO_3$ crystals, respectively. The O−O stretch is a broad feature at 857, 857, and 860 cm^{-1} for $K\_U_{22}PO_3$, $NaK\_U_{22}PO_3$, and $K\_U_{28}PO_3$ crystals, respectively. The spectrum of each crystal features bands in the 980−1100 cm^{-1} region that correspond to the $(HPO_3)^{2-}$ and TEAH groups. The bands for TEAH are strong in the spectrum for $K\_U_{28}PO_3$, and present, but weaker, in the cases of $K\_U_{22}PO_3$ and $NaK\_U_{22}PO_3$ (Figure S9, Supporting Information), consistent with the presence of bound tetraethylammonium cations in the crystalline structures.

UV−vis spectra (Figure S11, Supporting Information) were collected for crystals of $K\_U_{22}PO_3$, $NaK\_U_{22}PO_3$, and $K\_U_{28}PO_3$ using a Craig Instruments spectrometer.

3. RESULTS

3.1. Synthesis. The synthesis methods described herein provided crystals corresponding to the different clusters, $K\_U_{22}PO_3$, $NaK\_U_{22}PO_3$, and $K\_U_{28}PO_3$, as shown by X-ray diffraction (section 3.2). Raman spectra collected for crystals of each compound, for their mother solutions collected 3 days and 3 months after mixing, for the Na_2HPO_3 standard solution, and for crystals of $K\_U_{22}PO_3$, $NaK\_U_{22}PO_3$, and $K\_U_{28}PO_3$ all contain a P−H stretching mode in the range of 2330−2406 cm^{-1} (see the Supporting Information). Whereas the corresponding mode is at 2330 cm^{-1} for a solution of Na_2HPO_3, it is shifted to about 2380 cm^{-1} in the reaction solutions and into the range of 2392−2406 cm^{-1} in the crystals. The Raman spectra further reveal free peroxide O−O stretches at ∼876 cm^{-1}, as well as peroxide stretches at ∼860 cm^{-1}, consistent with coordination to uranyl. The Raman spectra demonstrate the presence of both free peroxide and phosphite in the reaction solution for at least 3 months, demonstrating that oxidation of phosphite was incomplete prior to cluster assembly and crystallization.

3.2. Structures. Single-crystal X-ray diffraction provided the structures of $U_{22}PO_3$ (for both crystals of $K\_U_{22}PO_3$ and $NaK\_U_{22}PO_3$) and $U_{28}PO_3$ (for $K\_U_{28}PO_3$) (Figures 1−3; Figures S2−S5, Supporting Information). Both clusters are chiral and occur as left- and right-handed varieties cocrystallized into a racemic crystal. Bond lengths, as well as the color of both the solution and the crystals, are consistent with all uranium being U^{6+}. Each U^{6+} cation is present as a typical $(UO_2)^{2+}$ uranyl ion with U−O bond lengths of ∼1.8 Å. Combinations of peroxo ligands, $(HPO_3)^{2-}$ ligands, and H_2O complete hexagonal or pentagonal bipyramids about the U^{6+} cations, with the apexes of these bipyramids corresponding to the O atoms of the uranyl ions. The $(HPO_3)^{2-}$ ligands exhibit typical

dx.doi.org/10.1021/ic3020817 | *Inorg. Chem.* 2013, 52, 337−345

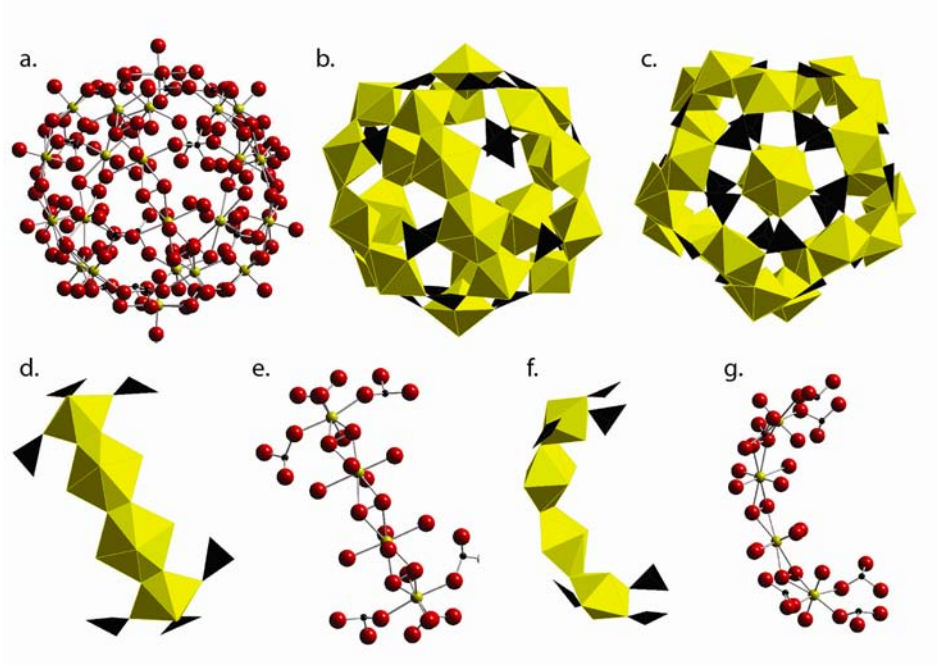

Figure 1. Ball-and-stick and polyhedral representations of $U_{22}PO_3$ (a–c) and selected fragments (d–g). Uranyl polyhedra and U^{6+} cations are shown in yellow, $(HPO_3)^{2-}$ ligands and P^{3+} cations are shown in black, and O atoms are illustrated as red spheres.

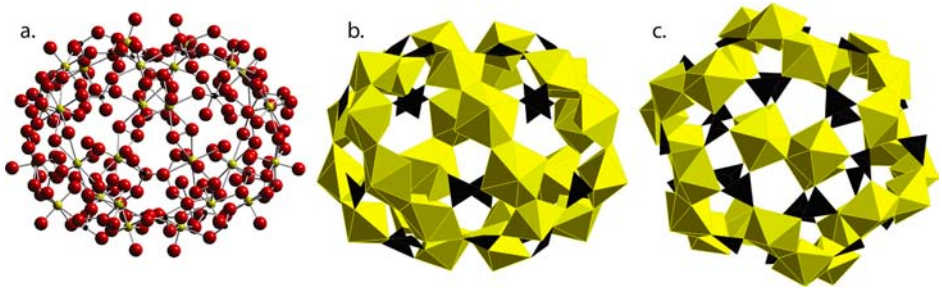

Figure 2. Ball-and-stick and polyhedral representations of $U_{28}PO_3$ (a–c). Legend as that in Figure 1.

triangular pyramidal geometries, with the H atom located at the apex of the pyramid.

The most prominent feature of $U_{22}PO_3$ is a belt that consists of four uranyl bipyramids (Figure 1). The bridges between the uranyl ions along the belt length are bidentate peroxo ligands, and the two central polyhedra are hexagonal bipyramids with two peroxo ligands in a *trans* configuration. The belt is terminated by a uranyl pentagonal bipyramid at either end, each of which contains only one bidentate peroxo ligand. In the case of the hexagonal bipyramids, one nonperoxide equatorial ligand corresponds to a monodentate $(HPO_3)^{2-}$, whereas the other is H_2O. The uranyl ions of the pentagonal bipyramids are coordinated by three $(HPO_3)^{2-}$ ligands, as well as the bidentate peroxo group. Five such belts of polyhedra form the walls of the cluster, where they are distributed about the equatorial and are connected by bridging $(HPO_3)^{2-}$ groups, giving C_5 symmetry (Figure 1b). The $U_{22}PO_3$ cluster is the second uranium peroxide cage cluster with C_5 symmetry, but otherwise is highly unique with the presence of belts of polyhedra, rather than rings, and uranyl pentagonal bipyramids.[56] Both poles of the cluster consist of a uranyl ion that is coordinated by five $(HPO_3)^{2-}$ ligands, giving pentagonal bipyramids. The cluster has a maximum diameter of 18.2 Å, as measured from the outer edges of bounding O atoms, and an inner diameter of 10.9 Å, measured between the inner edges of the bounding O atoms. Of the H atoms of the 20 $(HPO_3)^{2-}$ groups of $K\_U_{22}PO_3$, one is directed outside the cage cluster, and the other 19 extend into the interior of the cage (Figure S4, Supporting Information). In the case of $NaK\_U_{22}PO_3$, all 20 of the H atoms are directed inside the cage.

The uranyl polyhedra and $(HPO_3)^{2-}$ components of the cage cluster have a composition of $[(UO_2)_{22}(O_2)_{15}(HPO_3)_{20}(H_2O)_{10}]^{26-}$. In the case of $K\_U_{22}PO_3$, the crystal also contains disordered K cations that are located between the clusters (Figure 3a; Figure S5, Supporting Information), as well as some disordered tetraethylammonium cations (see section 3.3). The charge of the cluster in $NaK\_U_{22}PO_3$ is balanced in the crystal structure by the presence of five disordered Na cations located inside the cage (Figure 3b), additional disordered Na and K cations located between the clusters (Figure 3b; Figure S5, Supporting Information), and tetraethylammonium cations (see section 3.3). The distribution of Na^+ and K^+ cations in crystals of $NaK\_U_{22}PO_3$ gives fewer linkages between the $U_{22}PO_3$ clusters relative to $K\_U_{22}PO_3$ (Figure S5, Supporting Information). X-ray diffraction revealed electron density inside the cage that is consistent with partially disordered H_2O groups.

dx.doi.org/10.1021/ic3020817 | *Inorg. Chem.* 2013, 52, 337–345

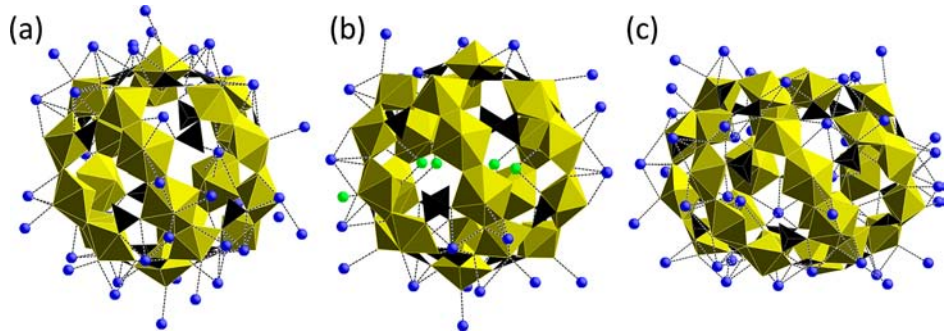

Figure 3. Polyhedral representations of clusters $K\_U_{22}PO_3$ (a), $NaK\_U_{22}PO_3$ (b), and $K\_U_{28}PO_3$ (c) showing the positions of K^+ and Na^+ ions. Uranyl polyhedra are shown in yellow; $(HPO_3)^{2-}$ polyhedra are shown in black; and K^+, Na^+, and O^{2-} ions are shown as blue, green, and red spheres, respectively.

The $U_{28}PO_3$ cluster contains belts of uranyl bipyramids that are identical to those in $U_{22}PO_3$. However, in this cluster, there are six such belts located about the equatorial of the cluster that are bridged by $(HPO_3)^{2-}$ ligands (Figure 2). The two poles of the cage cluster each correspond to two uranyl ions that share a bidentate peroxo ligand and that are coordinated by a total of six $(HPO_3)^{2-}$ ligands, giving two uranyl pentagonal bipyramids. There are 24 $(HPO_3)^{2-}$ groups in $U_{28}PO_3$, with 14 of the H atoms extending into the interior of the cage, and the other 10 directed outward (Figure S4, Supporting Information). The cluster has C_2 symmetry and a composition of $[(UO_2)_{28}(O_2)_{20}(HPO_3)_{24}(H_2O)_{12}]^{32-}$. X-ray diffraction revealed electron density inside the cage that is consistent with partially disordered H_2O groups as well as six K cations (Figure 3c). K cations are also located between the clusters (Figure 3c; Figure S5, Supporting Information), along with tetraethylammonium cations (see section 3.3). The cluster is larger than $U_{22}PO_3$, with a maximum diameter of 21.5 Å, as measured from the outer edges of bounding O atoms, and an inner free diameter of 11.6 Å, measured between the inner edges of the bounding O atoms.

The topologies of clusters $U_{22}PO_3$ and $U_{28}PO_3$ (Figure 4) are unique from those we reported earlier as they contain no four-, five-, or six membered rings of uranyl polyhedra, but rather are developed from four-membered belts of polyhedra. They are the first cage clusters with peroxide bridges between uranyl ions in a *trans* configuration in hexagonal bipyramids, the first to contain a uranyl pentagonal bipyramid with no peroxo ligands, and the first in which two uranyl pentagonal bipyramids are linked through a peroxo bridge. These clusters are also the first to occur as enantiomorphic pairs.

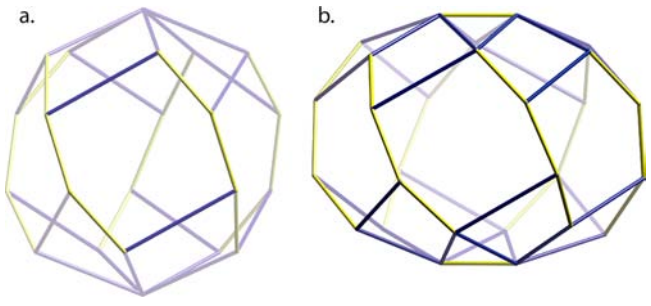

Figure 4. Graphical representations of the topologies of $U_{22}PO_3$ (a) and $U_{28}PO_3$ (b). All vertices of the graphs correspond to U^{6+} cations. Yellow lines connect vertices where their corresponding uranyl polyhedra share edges. Blue lines represent bridges through $(HPO_3)^{2-}$ ligands.

The $U_{22}PO_3$ and $U_{28}PO_3$ clusters contain 10 and 12 H_2O groups, respectively, each of which coordinate one uranyl ion at the equatorial vertex of a hexagonal bipyramid. The O···O separations between the O atom of the H_2O group and the nonbridging O atoms of two adjacent $(HPO_3)^{2-}$ groups are ~2.6–2.7 Å, indicating likely H bonds that extend between O atoms of two polyhedra in the cage cluster. Each of the terminal O atoms of the $(HPO_3)^{2-}$ groups likely accepts two H bonds, thereby providing linkages between adjacent belts of uranyl polyhedra in the cluster.

3.3. Composition of $U_{22}PO_3$ and $U_{28}PO_3$. The X-ray crystal structure analysis provided the formula $K_{14.73}[(UO_2)_{22}(O_2)_{15}(HPO_3)_{20}(H_2O)_{10}]^{11-}$ for crystals of $K\_U_{22}PO_3$. Considerable electron density between the clusters was left unassigned because of disorder. ICP-OES analyses of crystals of $K\_U_{22}PO_3$ gave U/P/K atomic percent ratios of 22.0:20.9:24.6, and $NaK\_U_{22}PO_3$ gave U/P/K/Na atomic percent ratios of 22.0:21.7:13.5:11.4, which indicates that a significant quantity of K and/or Na cations are unaccounted for in the crystal structure analyses. The Raman and IR spectra (Figures S7 and S9, Supporting Information) indicate the presence of tetraethylammonium groups in the crystals. C and N analyses gave mass percents of C and N in $K\_U_{22}PO_3$ crystals of C, 0.465%, and N, 0.044%. On the basis of the X-ray and TGA data (Figure S6, Supporting Information), there appears to be less than one tetraethylammonium cation per formula unit in $K\_U_{22}PO_3$. The composition of $K\_U_{22}PO_3$ is $K_x[N(CH_2CH_3)_4]_y[(UO_2)_{22}(O_2)_{15}(HPO_3)_{20}(H_2O)_{10}](H_2O)_n$, where $x \sim 25$, $y \sim 1$, $x + y = 26$, and $n \sim 36$. The composition of the $NaK\_U_{22}PO_3$ crystal is $K_xNa_y[N(CH_2CH_3)_4]_z[(UO_2)_{22}(O_2)_{15}(HPO_3)_{20}(H_2O)_{10}](H_2O)_n$, where $x \sim 13.5$, $y \sim 11.4$, $z \sim 1$, $x + y + z = 26$, and $n \sim 56$.

The X-ray crystal structure analysis provided the formula $K_{24}[(UO_2)_{28}(O_2)_{20}(HPO_3)_{24}(H_2O)_{12}]^{8-}$ for crystals of $U_{28}PO_3$, with disordered electron density between the clusters left unassigned. Atomic percentages for U/P/K from ICP-OES are 28.2:25.9:30.2, indicating additional K cations. The Raman and IR spectra (Figures S7 and S9, Supporting Information) indicate the presence of tetraethylammonium cations. C and N analyses gave the mass percents of C and N in $U_{28}PO_3$ crystals as C 1.792% and N 0.298%. The composition of crystals of $U_{28}PO_3$ is $K_x[N(CH_2CH_3)_4]_y[(UO_2)_{28}(O_2)_{20}(HPO_3)_{24}(H_2O)_{12}](H_2O)_n$, where $x \sim 30$, $y \sim 2$, $x + y = 32$, and $n \sim 57$.

3.4. SAXS and ESI-MS Studies of Dissolved $U_{22}PO_3$ and $U_{28}PO_3$. Here, we examine the fate of $U_{22}PO_3$ and $U_{28}PO_3$

dx.doi.org/10.1021/ic3020817 | *Inorg. Chem.* 2013, 52, 337–345

clusters upon dissolution into aqueous solution. Previous studies demonstrated that uranium peroxide clusters based on rings of polyhedra persist when dissolved in ultrapure water.[29,31,35,38,57] In the current study, $U_{22}PO_3$ crystals form first from the parent solution, followed by $U_{28}PO_3$ crystals after about 2 weeks. As the clusters in the parent solutions may be polydisperse, we first analyzed solutions created by dissolving crystals in aqueous solutions using SAXS and ESI-MS. The SAXS data (Figure 5) are consistent with the presence of a

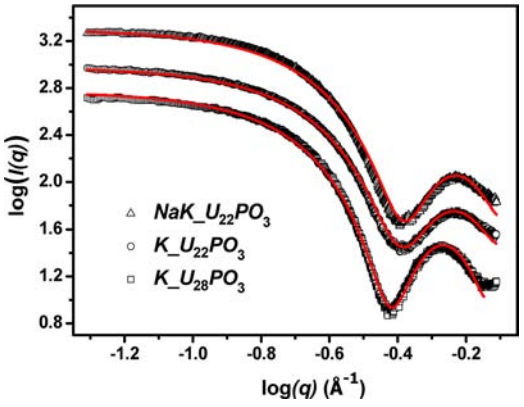

Figure 5. SAXS log–log plots (black) and corresponding model fits (red) for solutions created by dissolving single crystals of $NaK\_U_{22}PO_3$ and $K\_U_{28}PO_3$ in pure water, and $K\_U_{22}PO_3$ in 0.1 M Na_2HPO_3 aqueous solution.

monodisperse cluster in each solution. The data were fit using a sphere-shell model in each case, with outer and inner radii of the model being 9.1 and 5.5 Å for $U_{22}PO_3$ ($K\_U_{22}PO_3$ and $NaK\_U_{22}PO_3$) and 10.2 and 5.7 Å for $U_{28}PO_3$ ($K\_U_{28}PO_3$). These values are in agreement with dimensions from the crystallographic structures and are consistent with the persistence of $NaK\_U_{22}PO_3$ and $K\_U_{28}PO_3$ clusters upon dissolution in pure water, and $K\_U_{22}PO_3$ clusters in 0.1 M Na_2HPO_3 aqueous solution. ESI-MS data (Figure 6) indicate two types of clusters with a similar mass in a solution of $K\_U_{22}PO_3$, and a single cluster in a solution of $K\_U_{28}PO_3$. Deconvoluted spectra (Figure S12, Supporting Information) gave an average mass of 8700 Da for $K\_U_{22}PO_3$ and 10 400 Da for $K\_U_{28}PO_3$, respectively. The mass of the cluster, excluding counterions, is 8200 Da for $K\_U_{22}PO_3$ and 10 366 Da for $K\_U_{28}PO_3$. The ESI-MS data demonstrate that $U_{22}PO_3$ and $U_{28}PO_3$ persist upon dissolution in solution. The appearance of two clusters in the solution of $K\_U_{22}PO_3$ may be due to ion exchange between K^+ in the structure and Na^+ in the solvent. A similar ion exchange between K^+ and Na^+ was observed for the U_{28} cluster.[58]

3.5. Time-Resolved ESI-MS and SAXS Studies. ESI-MS and SAXS were used to monitor the self-assembly of clusters in solution. Time-resolved ESI-MS data collected after 1 h indicate only one cluster species (Figure 6), with a spectrum similar to that of the solution created by dissolving $K\_U_{28}PO_3$ crystals. Cluster $U_{28}PO_3$ forms within 1 h after mixing the reactants, although crystals of $U_{22}PO_3$ form first. Over time, the spectra remain similar, even after crystals of $U_{22}PO_3$ formed by the 15th day, and the corresponding spectrum is for a solution from which clusters of $U_{22}PO_3$ were growing. Cluster $U_{22}PO_3$ was not detected in mother solutions using ESI-MS, indicating that its concentration is below the detection limit, or that $U_{22}PO_3$ clusters are not present, perhaps because they

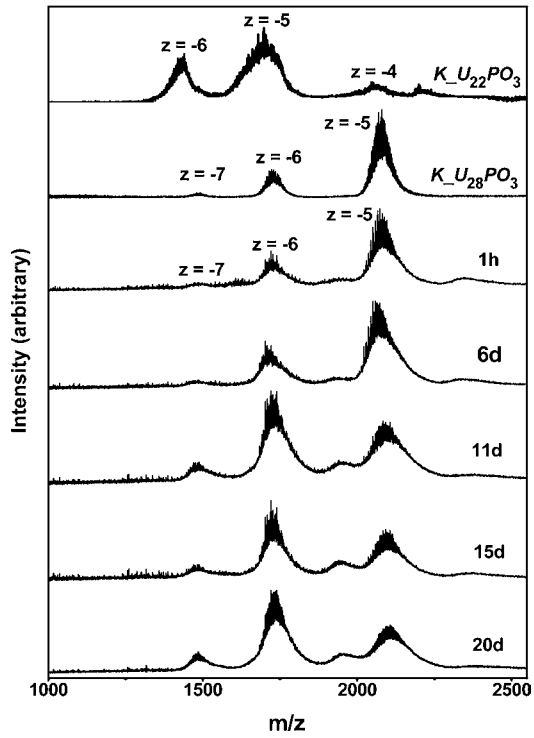

Figure 6. Electrospray ionization mass spectra (ESI-MS) for samples made by dissolving crystals of $K\_U_{22}PO_3$ in 1 mM Na_2HPO_3 aqueous solution and $K\_U_{28}PO_3$ in pure water, and samples made using aged reaction solutions of clusters $U_{22}PO_3$ and $U_{28}PO_3$.

disintegrated or precipitated following collection of the specimen. The yield of $U_{22}PO_3$ crystals was lower than that of $U_{28}PO_3$ crystals, consistent with a lower concentration of $U_{22}PO_3$ clusters in the solution.

Time-resolved SAXS data provide further insight into the self-assembly of clusters in solution (Figure 7). SAXS data were collected for samples of the mother solution collected over time, with the SAXS data collected immediately after sampling for the undiluted specimen. The SAXS data collected at different time intervals are compared to data collected for aqueous solutions into which crystals of one of $K\_U_{22}PO_3$ or $K\_U_{28}PO_3$ had been dissolved, as well as an aqueous solution into which a mixture of crystals of $K\_U_{22}PO_3$ and $K\_U_{28}PO_3$ was dissolved, with the crystals selected in the ratio of their abundance in the product.

The SAXS profile of the mother solution collected 1 h after combining the reactants is very similar to that of a mixture of dissolved $K\_U_{22}PO_3$ and $K\_U_{28}PO_3$ crystals, consistent with the presence of both of the $U_{22}PO_3$ and $U_{28}PO_3$ clusters in the solution, and consistent with less $U_{22}PO_3$ in solution than $U_{28}PO_3$. The scattering of the solution collected after 1 day is stronger than that of the 1 h old solution, indicating an increase in the concentration of clusters, although the average size of the cluster in solution does not appear to have changed. The SAXS patterns for solutions collected at 4, 11, and 13 days are essentially indistinguishable from that collected for the 1 day sample. On the 15th day, crystals of $U_{22}PO_3$ formed, and the SAXS profile for solutions collected after 15 and 20 days exhibit a shift to lower values of q (see inset in Figure 7), with the profile for the 20 day solution being similar to that collected for dissolved $U_{28}PO_3$ crystals. Upon crystallization of $U_{22}PO_3$, its concentration in solution is governed by the crystal solubility and presumably varies little. In contrast, the concentration of

dx.doi.org/10.1021/ic3020817 | Inorg. Chem. 2013, 52, 337–345

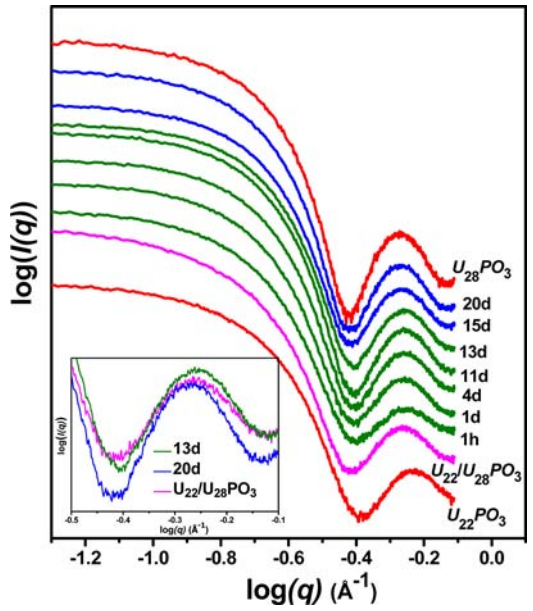

Figure 7. Selected SAXS log–log plots for aged reaction solutions of $U_{22}PO_3$ and $U_{28}PO_3$ clusters (green and blue), solutions created by dissolving one type of single crystals of $K\_U_{22}PO_3$ or $K\_U_{28}PO_3$ in an aqueous solution (red), and solution created by dissolving crystals of both $K\_U_{22}PO_3$ and $K\_U_{28}PO_3$ in an aqueous solution (pink). Inset: enlarged view of scattering profiles of 13th and 20th day reaction solutions, and solution created by dissolving both $K\_U_{22}PO_3$ and $K\_U_{28}PO_3$ crystals in an aqueous solution.

$U_{28}PO_3$ in solution probably increases as water evaporates. Crystals of $U_{28}PO_3$ form by 28 days.

3.6. Aqueous Solubility. Crystals of $NaK\_U_{22}PO_3$ and $K\_U_{28}PO_3$ both rapidly dissolved in ultrapure water at room temperature. In the course of preparing solutions for SAXS and ESI-MS measurements, we observed that crystals of $K\_U_{22}PO_3$ failed to dissolve in ultrapure water, even after prolonged soaking. However, crystals of $K\_U_{22}PO_3$ readily dissolved in an aqueous solution of 1 mM Na_2HPO_3.

4. DISCUSSION

The mineral studtite, $[(UO_2)(O_2)(H_2O)_2](H_2O)_2$, contains uranyl ions that are bridged by peroxo ligands in a *trans* arrangement, with the other two ligands of each hexagonal bipyramid being H_2O groups in a *trans* configuration.[59,60] The infinite chains of hexagonal bipyramids are linked into an extended structure through H bonds only. The U–(O_2)–U dihedral angles in the studtite chain are 140.2°. The belts of uranyl polyhedra in $U_{22}PO_3$ and $U_{28}PO_3$ are similar to the studtite chain, but rather than being corrugated, as in studtite, the U–(O_2)–U dihedral angles are cooperative, resulting in curvature (Figure 1f,g). The U–(O_2)–U dihedral angles range from 133.1 to 145.7° in these clusters, providing the curvature that facilitates cage cluster formation rather than an extended structure.

Studtite rapidly precipitates where uranyl ions and peroxide are at sufficient concentrations in acidic to circum-neutral aqueous solutions. We expect that fragments of the studtite chain preform in solution over a broad range of conditions, although more alkaline solutions favor rings of uranyl polyhedra that include hydroxyl bridges, as found in many of the clusters we reported earlier. Under circum-neutral to acidic conditions, none of the cage clusters we have grown contain hydroxyl bridges, and rings of uranyl polyhedra only form cage clusters either by sharing three peroxide edges per polyhedron or through bridges other than peroxide or hydroxyl (such as oxalate or pyrophosphate). By adjusting the pH into the weakly acidic range in this case, we precluded hydroxyl bridges between uranyl polyhedra. Providing only $(HPO_3)^{2-}$ and peroxide as bridges has stabilized clusters containing studtite-like belts, rather than rings. The $U_{22}PO_3$ and $U_{28}PO_3$ clusters demonstrate that judicious selection of bridging oxyanions can favor the assembly of uranyl peroxo cage clusters with unique topological and structural features.

Cage clusters built from uranyl polyhedra represent a unique family of polyoxometalates, not only because they contain actinides but also because they contain the linear $(UO_2)^{2+}$ dioxo cations. The uranyl ions are locally perpendicular to the cluster walls, and the "yl" atoms passivate the inner and outer surfaces of the cage clusters. All of these cage clusters carry a negative charge that is neutralized in the solid state by closely associated alkali or alkaline earth cations. Typically, these are located both within and between the cage clusters.

Alkali cations inside cage clusters of uranyl polyhedra are normally located inside four-, five-, or six-membered rings of uranyl polyhedra,[34,35,38–40,58,61] and specific building blocks have a strong affinity for specific alkali cations.[44] DFT calculations have demonstrated that the size of the counter-cation affects the dihedral angle of the U–(O_2)–U linkage, which is thought to be the major feature that causes uranyl polyhedra to self-assemble into clusters.[44,45] However, there are no obvious positional relationships between Na^+ and/or K^+ ions and the belts of uranyl polyhedra in clusters $U_{22}PO_3$ and $U_{28}PO_3$, which suggests different assembly mechanisms, in contrast to previously described clusters.

It is remarkable that the aqueous solubilities of $NaK\_U_{22}PO_3$ and $K\_U_{28}PO_3$ are markedly higher in ultrapure water than crystals of $K\_U_{22}PO_3$, although crystals of $K\_U_{22}PO_3$ readily dissolve in 1 mM Na_2HPO_3. Our several years of experience with uranyl peroxide cage clusters indicates that most are readily soluble in pure water.[31,35,38,39] Given that the topologies of the cages of $NaK\_U_{22}PO_3$ and $K\_U_{22}PO_3$ are identical, and that these share several commonalities with $K\_U_{28}PO_3$, it is interesting to examine factors that could result in their very different solubilities in ultrapure water.

The uranyl phosphite portions of the cages of $NaK\_U_{22}PO_3$ and $K\_U_{22}PO_3$ are almost identical. All of the H atoms of the $(HPO_3)^{2-}$ groups extend toward the interior of the cluster in the case of $NaK\_U_{22}PO_3$, and all but one do likewise in $K\_U_{22}PO_3$. The major difference is that there are no counterions inside $K\_U_{22}PO_3$, whereas there are five Na cations within the $NaK\_U_{22}PO_3$ cage. The average charge densities, obtained by dividing the total charge of the cluster by the number of non-H atoms, are 0.140 for $K\_U_{22}PO_3$, 0.110 for $NaK\_U_{22}PO_3$, and 0.109 for $K\_U_{28}PO_3$. Higher charge densities suggest stronger interactions between the anionic cluster and counterions in solution, and lower aqueous solubility because counterions bridge clusters to form a solid. On the basis of charge density, one would expect $NaK\_U_{22}PO_3$ and $K\_U_{28}PO_3$ to be more soluble than $K\_U_{22}PO_3$, as observed.

Given that the $NaK\_U_{22}PO_3$, $K\_U_{28}PO_3$, and $K\_U_{22}PO_3$ clusters are cages that interact with counterions outside the cage, we calculated the average surface charge of the cluster, ignoring counterions located outside of the cage, and distributing the net charge of the cluster evenly over a sphere

dx.doi.org/10.1021/ic3020817 | *Inorg. Chem.* 2013, 52, 337–345

with a diameter equal to the distance between the outer edges of bounding O atoms. This gives average surface charges of −2.5 nm^{-2} for $K\_U_{22}PO_3$, −2.0 nm^{-2} for $NaK\_U_{22}PO_3$, and −1.8 nm^{-2} for $K\_U_{28}PO_3$. $K\_U_{22}PO_3$ is differentiated from $NaK\_U_{22}PO_3$ and $K\_U_{28}PO_3$ in that its average surface charge is 25−39% larger. $K\_U_{22}PO_3$ dissolves readily in a solution of 1 mM Na_2HPO_3, perhaps because Na cations move inside the cage, thereby reducing the average surface charge of the cluster.

■ ASSOCIATED CONTENT

Supporting Information

Figures showing crystals; polyhedral and ball-and-stick representations; thermograms; IR, Raman, UV-vis, and ESI-MS spectra; and PXRD patterns and Tables containing crystal and structure data, final coordinates and equivalent isotropic displacement parameters, and bond distances and angles. This material is available free of charge via the Internet at http://pubs.acs.org.

■ AUTHOR INFORMATION

Corresponding Author

*E-mail: pburns@nd.edu.

Notes

The authors declare no competing financial interest.

■ ACKNOWLEDGMENTS

This material is based upon work supported as part of the Materials Science of Actinides Center, an Energy Frontier Research Center funded by the U.S. Department of Energy, Office of Science, Office of Basic Energy Sciences, under Award Number DE-SC0001089.

■ REFERENCES

(1) Pope, M. T.; Muller, A. *Angew. Chem., Int. Ed. Engl.* **1991**, *30*, 34.
(2) Long, D. L.; Tsunashima, R.; Cronin, L. *Angew. Chem., Int. Ed.* **2010**, *49*, 1736.
(3) Hasenknopf, B.; Micoine, K.; Lacote, E.; Thorimbert, S.; Malacria, M.; Thouvenot, R. *Eur. J. Inorg. Chem.* **2008**, 5001.
(4) Long, D. L.; Burkholder, E.; Cronin, L. *Chem. Soc. Rev.* **2007**, *36*, 105.
(5) Muller, A.; Peters, F.; Pope, M. T.; Gatteschi, D. *Chem. Rev.* **1998**, *98*, 239.
(6) Burns, P. C. *Mineral. Mag.* **2011**, *75*, 1.
(7) Liu, T. *Langmuir* **2010**, *26*, 9202.
(8) Biswas, B.; Mougel, V.; Pecaut, J.; Mazzanti, M. *Angew. Chem., Int. Ed.* **2011**, *50*, 5745.
(9) Qiu, J.; Burns, P. C. *Chem. Rev.* **2012**, in press.
(10) Nyman, M.; Burns, P. C. *Chem. Soc. Rev.* **2012**, *41*, 7354.
(11) Soderholm, L.; Almond, P. M.; Skanthakumar, S.; Wilson, R. E.; Burns, P. C. *Angew. Chem., Int. Ed.* **2008**, *47*, 298.
(12) Mokry, L. M.; Dean, N. S.; Carrano, C. J. *Angew. Chem., Int. Ed. Engl.* **1996**, *35*, 1497.
(13) Takao, S.; Takao, K.; Kraus, W.; Ernmerling, F.; Scheinost, A. C.; Bernhard, G.; Hennig, C. *Eur. J. Inorg. Chem.* **2009**, 4771.
(14) Salmon, L.; Thuery, P.; Ephritikhine, M. *Polyhedron* **2004**, *23*, 623.
(15) Coronado, E.; Gomez-Garcia, C. J. *Chem. Rev.* **1998**, *98*, 273.
(16) Morss, L. R.; Edelstein, N. M.; Fuger, J.; Katz, J. J. *The Chemistry of the Actinide and Transactinide Elements*; Springer: Dordrecht, 2006.
(17) Knope, K. E.; Wilson, R. E.; Vasiliu, M.; Dixon, D. A.; Soderholm, L. *Inorg. Chem.* **2011**, *50*, 9696.
(18) Diwu, J.; Good, J. J.; DiStefano, V. H.; Albrecht-Schmitt, T. E. *Eur. J. Inorg. Chem.* **2011**, 1374.
(19) Diwu, J.; Wang, S.; Albrecht-Schmitt, T. E. *Inorg. Chem.* **2012**, *51*, 4088.
(20) Duval, P. B.; Burns, C. J.; Clark, D. L.; Morris, D. E.; Scott, B. L.; Thompson, J. D.; Werkema, E. L.; Jia, L.; Andersen, R. A. *Angew. Chem., Int. Ed.* **2001**, *40*, 3358.
(21) Berthet, J. C.; Thuery, P.; Ephritikhine, M. *Chem. Commun.* **2005**, 3415.
(22) Berthet, J. C.; Thuery, P.; Ephritikhine, M. *Inorg. Chem.* **2010**, *49*, 8173.
(23) Nocton, G.; Pecaut, J.; Filinchuk, Y.; Mazzanti, M. *Chem. Commun.* **2010**, *46*, 2757.
(24) Nocton, G.; Burdet, F.; Pecaut, J.; Mazzanti, M. *Angew. Chem., Int. Ed.* **2007**, *46*, 7574.
(25) Lundgren, G. *Ark. Kemi* **1952**, *5*, 349.
(26) Moisan, L.; Le Borgne, T.; Thuery, P.; Ephritikhine, M. *Acta Crystallogr., Sect. C: Cryst. Struct. Commun.* **2002**, *58*, m98.
(27) Burns, P. C.; Kubatko, K. A.; Sigmon, G.; Fryer, B. J.; Gagnon, J. E.; Antonio, M. R.; Soderholm, L. *Angew. Chem., Int. Ed.* **2005**, *44*, 2135.
(28) Forbes, T. Z.; McAlpin, J. G.; Murphy, R.; Burns, P. C. *Angew. Chem., Int. Ed.* **2008**, *47*, 2824.
(29) Ling, J.; Qiu, J.; Sigmon, G. E.; Ward, M.; Szymanowski, J. E. S.; Burns, P. C. *J. Am. Chem. Soc.* **2010**, *132*, 13395.
(30) Ling, J.; Qiu, J.; Szymanowski, J. E. S.; Burns, P. C. *Chem.—Eur. J.* **2011**, *17*, 2571.
(31) Ling, J.; Wallace, C. M.; Szymanowski, J. E. S.; Burns, P. C. *Angew. Chem., Int. Ed.* **2010**, *49*, 7271.
(32) Sigmon, G.; Ling, J.; Unruh, D. K.; Moore-Shay, L.; Ward, M.; Weaver, B.; Burns, P. C. *J. Amer. Chem .Soc.* **2009**, *131*, 16648.
(33) Sigmon, G. E.; Unruh, D. K.; Ling, J.; Weaver, B.; Ward, M.; Pressprich, L.; Simonetti, A.; Burns, P. C. *Angew. Chem., Int. Ed.* **2009**, *48*, 2737.
(34) Sigmon, G. E.; Weaver, B.; Kubatko, K. A.; Burns, P. C. *Inorg. Chem.* **2009**, *48*, 10907.
(35) Unruh, D. K.; Burtner, A.; Pressprich, L.; Sigmon, G.; Burns, P. C. *Dalton Trans.* **2010**, *39*, 5807.
(36) Sigmon, G.; Burns, P. C. *J. Am. Chem. Soc.* **2011**, *133*, 9137.
(37) Unruh, D. K.; Ling, J.; Qiu, J.; Pressprich, L.; Baranay, M.; Ward, M.; Burns, P. C. *Inorg. Chem.* **2011**, *50*, 5509.
(38) Qiu, J.; Ling, J.; Sui, A.; Szymanowski, J. E. S.; Simonetti, A.; Burns, P. C. *J. Am. Chem. Soc.* **2012**, *134*, 1810.
(39) Ling, J.; Qiu, J.; Burns, P. C. *Inorg. Chem.* **2012**, *51*, 2403.
(40) Ling, J.; Ozga, M.; Stoffer, M.; Burns, P. C. *Dalton Trans.* **2012**, *41*, 7278.
(41) Burns, P. C.; Ewing, P. C.; Miller, M. L. *J. Nucl. Mater.* **1997**, *245*, 1.
(42) Burns, P. C. *Can. Mineral.* **2005**, *43*, 1839.
(43) Burns, P. C.; Miller, M. L.; Ewing, R. C. *Can. Mineral.* **1996**, *34*, 845.
(44) Miro, P.; Pierrefixe, S.; Gicquel, M.; Gil, A.; Bo, C. *J. Am. Chem. Soc.* **2010**, *132*, 17787.
(45) Vlaisavljevich, B.; Gagliardi, L.; Burns, P. C. *J. Am. Chem. Soc.* **2010**, *132*, 14503.
(46) Doran, M.; Walker, S. M.; O'Hare, D. *Chem. Commun.* **2001**, 1988.
(47) Villa, E. M.; Wang, S.; Alekseev, E. V.; Depmeier, W.; Albrecht-Schmitt, T. E. *Eur. J. Inorg. Chem.* **2011**, 3749.
(48) Mandal, S.; Chandra, M.; Natarajan, S. *Inorg. Chem.* **2007**, *46*, 7935.
(49) Villa, E. M.; Marr, C. J.; Jouffret, L. J.; Alekseev, E. V.; Depmeier, W.; Albrecht-Schmitt, T. E. *Inorg. Chem.* **2012**, *51*, 6548.
(50) Cross, J. N.; Villa, E. M.; Wang, S.; Juan, D.; Polinski, M. J.; Albrecht-Schmitt, T. E. *Inorg. Chem.* **2012**, *51*, 8419.
(51) Bayot, D.; Tinant, B.; Devillers, M. *Inorg. Chem.* **2004**, *43*, 5999.
(52) Sheldrick, G. M. *SADABS: Bruker AXS Area Detector Scaling and Adsorption*, version 2008/1; University of Göttingen: Göttingen, Germany, 2008.
(53) Sheldrick, G. M. *SHELXTL*; Bruker AXS, Inc.: Madison, WI, 1996.
(54) Burns, P. C.; Ewing, R. C.; Hawthorne, F. C. *Can. Mineral.* **1997**, *35*, 1551.

(55) Fenn, J. B.; Mann, M.; Meng, C. K.; Wong, S. F.; Whitehouse, C. M. *Science* **1989**, *246*, 64.
(56) Unruh, D. K.; Ling, J.; Qiu, J.; Pressprich, L.; Baranay, M.; Ward, M.; Burns, P. C. *Inorg. Chem.* **2011**, *50*, 5509.
(57) Armstrong, C. R.; Nyman, M.; Shvareva, T.; Sigmon, G. E.; Burns, P. C.; Navrotsky, A. *Proc. Natl. Acad. Sci. U.S.A.* **2012**, *109*, 1874.
(58) Nyman, M.; Rodriguez, M. A.; Alam, T. M. *Eur. J. Inorg. Chem.* **2011**, 2197.
(59) Burns, P. C.; Hughes, K. A. *Am. Mineral.* **2003**, *88*, 1165.
(60) Kubatko, K. A. H.; Helean, K. B.; Navrotsky, A.; Burns, P. C. *Science* **2003**, *302*, 1191.
(61) Gil, A.; Karhanek, D.; Miro, P.; Antonio, M. R.; Nyman, M.; Bo, C. *Chem.—Eur. J.* **2012**, *18*, 8340.